AIAA JOURNAL
Vol. 38, No. 3, March 2000

Higher-Order Finite Element for Sandwich Plates

S. Oskooei* and J. S. Hansen†
University of Toronto, Downsview, Ontario M3H 5T6, Canada

A finite element model for the analysis of sandwich plates with laminated composites facesheets is developed. In the model, the facesheets are represented as Reissner–Mindlin plates and the core is modeled as a three-dimensional continuum in which the through-thickness representation of the displacement fields is of a mixed form. That is, the u and v deflections are cubic functions of z, whereas w is a quadratic function of z. This representation allows accurate modeling of a wide range of core types (honeycomb and foam) and in particular core materials that have low in-plane stiffness compared to the transverse stiffness. Also, these through-thickness trial functions allow an accurate representation of transverse shear and normal stresses. The presented model provides a powerful general tool for the analysis of sandwich plates; transverse normal and shear stresses can be determined explicitly at the core/facesheet interface. Also, because of the core model adopted, good accuracy is obtained when large differences in transverse vs in-plane core stiffness is present, as well as for cases in which the core stiffness changes rapidly in the plane of the plate. The capability of the model is illustrated with several examples.

Nomenclature

E_{ii}	= Young's modulus in ii direction
$\boldsymbol{f}$	= applied force vector
G_{ij}	= shear modulus in ij direction
$\bar{Q}_{ij}$	= lamina stiffness parameter
t_b	= bottom facesheet thickness
t_c	= core thickness
t_t	= top facesheet thickness
t_0	= half-core thickness
t_1	= $t_0 + t_b$
t_2	= $t_0 + t_t$
U	= strain energy
u, v, w	= displacement in x, y, and z, respectively
W	= work done by external forces
γ_{ij}	= shear strain in ij direction
ϵ_{ij}	= strain in ij direction
σ_{ij}	= stress in ij direction
Φ	= potential energy
Ψ_x, Ψ_y	= plate rotation about x and y direction

I. Introduction

A SANDWICH structural design may be selected to satisfy various engineering objectives, for example, improved buoyancy, increased local thickness, achieving a specific thermal conductivity, or enhanced acoustic properties. However, the most common structural reason is to separate the thin stiff facesheets and thereby increase flexural stiffness and strength without significantly adding plate mass. As an illustration, the introduction of a honeycomb core into a solid material so that the thickness is increased by a factor of four increases the bending stiffness 37 times and strength 9 times with only a 6% increase in weight.[1] Such designs yield very high stiffness to weight as well as strength to weight ratios and are, therefore, extremely popular in high-performance and aerospace vehicles.

The facesheet/core components of a sandwich construction typically have very different physical characteristics, and as such the analysis of sandwich plates or shells requires a degree of sophistication that is greater than that of classical or Reissner–Mindlin plate/shell theory. Thus, sandwich plate problems have attracted the attention of many researchers. Reissner[2] developed a sandwich plate model as a combination of two facesheets that provide only membrane stiffness separated by a core that offered only transverse shear stiffness; although the through-thickness stiffness of the core is not explicitly included, it is assumed the core inhibits relative through-thickness deformation of the facesheets. This model sets the standard for most sandwich plate/shell models. Allen[3] and Plantema[4] assumed the in-plane displacement of the core through its thickness is linear; that is, plane sections of the core remain plane after deformation. A sandwich beam model that allows anisotropic and composite skins and a core with negligible in-plane stiffness was treated by Holt and Webber,[5] Pearce,[6] and Monforton and Ibrahim.[7] Sandwich structures in which the normal deflections of the skins are independent variables were considered by Ojalvo,[8] although this analysis ignores the normal stress between the skin and core. Frostig et al.[9] studied the behavior of nonsymmetric sandwich beams using a superposition approach. Frostig et al.[10] take into account higher-order effects resulting from the nonlinearity of the core displacement field, whereas in Ref. 11 the work is extended to sandwich panels. The theory uses classical plate theory for the skins and a three-dimensional elasticity theory for the core. Frostig and Baruch[12] enhanced their model to investigate the localized load effects of sandwich panels with a flexible core. However, because of problem complexity, in both models the in-plane rigidity of the core is ignored. Higher-order plate theory as used by Reddy[13,14] allows nonlinear distortions of the core, overcoming the shortcomings encountered in classical theories. Robbins and Reddy[15] developed the concept of layerwise laminates to model thick composites. In higher-order theories, it is assumed the core thickness remains unchanged, which implies an incompressible core, and therefore, both skins move in unison in the through-thickness direction. This may represent a severe restriction for problems involving point loads or spatially rapidly varying loads. Furthermore, higher-order theory imposes that the strain fields be continuous and differentiable with respect to z; this may lead to physically unrealistic results at laminate ply interfaces where certain strain components may not be continuous. Thybo Thomsen[16] used an improved elastic foundation model that extends models incorporating a Winkler foundation model by accounting for the existence of shear interaction between the facesheets and the core. This solution is applicable only to problems with concentrated loads or distributed loads that are applied over a very small area. Thybo Thomsen[17] then includes the interaction between the two facesheets and transverse shear effects in the facesheets in his next work.

Although the idea of designing a strong, durable, and lightweight structure is widely accepted, the design tools are not well established. That is, many of the existing sandwich models ignore transverse normal and/or shear stresses even though these stresses are crucial in failure analyses. The effects of such stresses are

Received 20 October 1997; revision received 21 July 1999; accepted for publication 6 August 1999.

*Graduate Student, Institute for Aerospace Studies, 4925 Dufferin Street.
†Professor, Institute for Aerospace Studies, 4925 Dufferin Street.

determined using various postprocessing techniques. As noted by Thybo Thomsen,[16] an accurate resolution of transverse normal and/or shear stresses becomes crucial for sandwich structures that are subjected to spatially rapidly varying loads or when core stiffness properties change rapidly. The present model takes the core modeling ideas of Frostig et al.,[10] Frostig and Baruch,[11] and Thybo Thomsen[16] and combines them with a facesheet model that includes transverse shear effects. Furthermore, these modeling ideas are used to develop a finite element formulation that should give accurate modeling with a flexibility to analyze a broad range of sandwich plate problems. To include facesheet shear-deformation effects, the facesheet model uses Reissner–Mindlin laminated plate theory. Shear-locking difficulties resulting from the finite element representation of the facesheets are avoided by adopting bicubic Lagrange trial functions[18] for the displacements u, v, and w. Note that, by explicitly including transverse shear effects in the facesheets, stress and delamination analyses of composite facesheets may be addressed directly, and it is expected that more accurate results would be obtained. The core is considered to be a three-dimensional material in which the transverse normal and shear stiffness are much more important (within the context of a sandwich analysis) than the in-plane properties. Therefore, following models of Refs. 10, 11, and 16 in which the core in-plane properties are assumed negligible, it is assumed that u and v are cubic polynomials in z, whereas w is quadratic in z. The present model does not assume that the core in-plane properties are negligible; however, this particular representation of u, v, and w will allow the effects of negligible properties when appropriate. For example, the present model has the capability of reducing to the model in Refs. 10 and 11 by setting the in-plane core stiffnesses E_{11}, E_{22}, and G_{12} to zero. In the element development, through-thickness integration of the strain energy is completed analytically; this leads to computational efficiency and gives the appearance of a two-dimensional finite element procedure. The formulation yields the result that the through-thickness normal (peeling stress) and shear stress are continuous functions of z. Hence, at any point through the core, stress information is available without additional through-thickness interpolation; this leads to a more accurate stress analysis with direct implications for failure prediction.

The example results presented demonstrate the accuracy of the model. It will be shown that this finite element capability provides a powerful and flexible tool for the analysis of sandwich plates. Thus, the range of applications for this tool varies from specially designed material for aerospace applications to thick sandwich slabs used in civil engineering structures.

II. Mathematical Model

The intent in the current formulation is to use an effective three-dimensional finite element model but with only a few elements through the thickness. Also, the through-thickness integration will be carried out in closed form, which will speed up calculations and simultaneously give the model a two-dimensional appearance.

For the facesheets, it was felt important to include transverse shear effects to allow the capture of facesheet delamination and facesheet/core disbonding. Thus, the facesheets are modeled using through-thickness trial functions that are consistent with Reissner–Mindlin plate theory. It should be noted, however, that the displacement field representation used is not that typically associated with the Reissner–Mindlin model (u_0, v_0, w_0, Ψ_x, Ψ_y). Rather, for the top and bottom facesheets, the variables used are (u_t, u_b, v_t, v_b, w_b) and (u_t, u_b, v_t, v_b, w_t), respectively, where the subscripts, t and b are the top or bottom of the particular facesheet under consideration. It may be seen that this representation is completely analogous to the standard representation, but it allows a simpler through-thickness assembly using standard finite element ideas. Furthermore, the advantage of the standard representation that the membrane and bending problems uncouple (linear analysis, symmetric laminate) is a nonquestion inasmuch as the membrane bending of a facesheet will never uncouple because the reference surface for the analysis is the sandwich middle surface.

The core trial functions are also chosen to yield special characteristics. In the work mentioned earlier[10,11] it was noted that for many sandwich core materials the in-plane normal and shear stiffnesses E_{xx}, E_{yy}, and E_{xy} are much less than the through-thickness counterparts E_{zz}, E_{yz}, and E_{xz}; thus, the assumption was made that $E_{xx} = E_{yy} = E_{xy} \approx 0$. This simplifies the analysis considerably but perhaps more importantly dictates a particular form for the core displacement field. That is, u and v must be cubic functions of z whereas w is a quadratic function of z; there must be this difference to allow the neglect of the energy associated with E_{xx}, E_{yy}, and E_{xy}. It is true that foam core materials do not exhibit the difference in stiffnesses noted earlier; however, it is also true that E_{xx}, E_{yy}, and E_{xy} of foam cores are much less than the corresponding stiffnesses for the facesheets and, therefore, the core strain energy associated with E_{xx}, E_{yy}, and E_{xy} is small compared to the corresponding facesheet strain energy. This again leads to the conclusion that the core stiffnesses E_{xx}, E_{yy}, and E_{xy} may be ignored with the preceding implications for the through-thickness form of the trial functions for u, v, and w. Thus, in the current finite element model, the core u, v, and w are modeled in the form just mentioned. Note that in the present formulation the core stiffnesses E_{xx}, E_{yy}, and E_{xy} are not set to zero as in Refs. 9–12 and 16 but are included; however, by adopting the trial function in the form indicated it will allow the strain energy corresponding to these terms to have negligible effect if it is appropriate. That is, the use of these trial functions will not induce artificial stiffening.

Based on the preceding discussion, the through-thickness nodal arrangement is determined as shown in Fig. 1. The nodal degrees of freedom associated with each node are as indicated.

Next, the in-plane (x, y) trial functions are considered. One of the simplest methods to overcome shear locking is using higher-order approximating polynomials[18]; furthermore, higher-order trial functions also lead to extremely accurate formulations. Therefore, bicubic trial functions in (x, y) were adopted to model u, v, and w in facesheets. From compatibility considerations this in turn dictates bicubic trial functions in (x, y) for u, v, and w in the core. The node layout in the plane is also shown in Fig. 1. The trial functions adopted for the displacements take following form.

Bottom facesheet:

$$u(x, y, z) = a_0(x, y) + a_1(x, y)z$$

$$v(x, y, z) = b_0(x, y) + b_1(x, y)z, \qquad w(x, y) = k_0(x, y) \tag{1}$$

Core:

$$u(x, y, z) = c_0(x, y) + c_1(x, y)z + c_2(x, y)z^2 + c_3(x, y)z^3$$

$$v(x, y, z) = d_0(x, y) + d_1(x, y)z + d_2(x, y)z^2 + d_3(x, y)z^3$$

$$w(x, y) = e_0(x, y) + e_1(x, y)z + e_2(x, y)z^2 \tag{2}$$

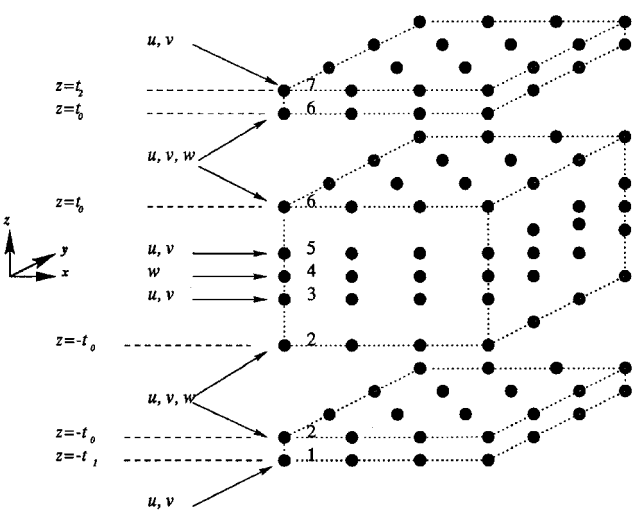

Fig. 1 Element schematic.

Top facesheet:

$$u(x, y, z) = f_0(x, y) + f_1(x, y)z$$

$$v(x, y, z) = g_0(x, y) + g_1(x, y)z, \qquad w(x, y) = h_0(x, y) \tag{3}$$

where

$$a_0, a_1, b_0, b_1, k_0, c_0, c_1, c_2, c_3, d_0, d_1, d_2, d_3, e_0, e_1, e_2, f_0, f_1, g_0, g_1, h_0 \tag{4}$$

are bicubic functions of x and y.

Considering only linear terms, the strain-displacement relation for the top or bottom facesheets is

$$\begin{bmatrix} \epsilon_x \\ \epsilon_y \\ \gamma_{yz} \\ \gamma_{xz} \\ \gamma_{xy} \end{bmatrix} = \begin{bmatrix} \frac{\partial}{\partial x} & 0 & 0 \\ 0 & \frac{\partial}{\partial y} & 0 \\ 0 & \frac{\partial}{\partial z} & \frac{\partial}{\partial y} \\ \frac{\partial}{\partial z} & 0 & \frac{\partial}{\partial x} \\ \frac{\partial}{\partial y} & \frac{\partial}{\partial x} & 0 \end{bmatrix} \begin{bmatrix} u \\ v \\ w \end{bmatrix} \tag{5}$$

The elasticity matrix C for a facesheet lamina is

$$\begin{bmatrix} \bar{Q}_{11} & \bar{Q}_{12} & 0 & 0 & \bar{Q}_{16} \\ & \bar{Q}_{22} & 0 & 0 & \bar{Q}_{26} \\ & & \bar{Q}_{44} & \bar{Q}_{45} & 0 \\ & & & \bar{Q}_{55} & 0 \\ \text{sym} & & & & \bar{Q}_{66} \end{bmatrix} \tag{6}$$

where $\bar{Q}_{ij}$ are the lamina stiffness parameters.[19]

For the core, the strain-displacement relation is

$$\begin{bmatrix} \epsilon_x \\ \epsilon_y \\ \epsilon z \\ \gamma_{yz} \\ \gamma_{xz} \\ \gamma_{xy} \end{bmatrix} = \begin{bmatrix} \frac{\partial}{\partial x} & 0 & 0 \\ 0 & \frac{\partial}{\partial y} & 0 \\ 0 & 0 & \frac{\partial}{\partial z} \\ 0 & \frac{\partial}{\partial z} & \frac{\partial}{\partial y} \\ \frac{\partial}{\partial z} & 0 & \frac{\partial}{\partial x} \\ \frac{\partial}{\partial y} & \frac{\partial}{\partial x} & 0 \end{bmatrix} \begin{bmatrix} u \\ v \\ w \end{bmatrix} \tag{7}$$

and the elasticity matrix C for a lamina is

$$\begin{bmatrix} \bar{Q}_{11} & \bar{Q}_{12} & \bar{Q}_{13} & 0 & 0 & \bar{Q}_{16} \\ & \bar{Q}_{22} & \bar{Q}_{23} & 0 & 0 & \bar{Q}_{26} \\ & & \bar{Q}_{33} & 0 & 0 & \bar{Q}_{36} \\ & & & \bar{Q}_{44} & \bar{Q}_{45} & 0 \\ & & & & \bar{Q}_{55} & 0 \\ \text{sym} & & & & & \bar{Q}_{66} \end{bmatrix} \tag{8}$$

Note that no shear correction factors have been included. The rational for this is twofold: For the face sheets it is felt that shear deformation does not contribute significantly to the response; for the core it is felt that the displacement field inherently models the the shear deformation accurately.

III. Finite Element Formulation

The potential energy of the plate is

$$\Phi = U - W = \frac{1}{2}\int_v \{\bar{\sigma}\}\{\bar{\epsilon}\}^T \, \mathrm{d}v - \int_s \{\bar{f}\}^T \{\bar{u}\} \, \mathrm{d}s \tag{9}$$

where v is the plate volume and s is its surface; $\{\bar{\sigma}\}$ and $\{\bar{\epsilon}\}$ are the full three-dimensional set of elastic stresses and strains, respectively; $\{\bar{u}\}$ are the displacements; and $\{\bar{f}\}$ are the surface tractions.

The present development is restricted to linear geometric and linear elastic considerations. Thus,

$$\{\bar{\sigma}\} = [\bar{Q}]\{\bar{\epsilon}\} \tag{10}$$

where $[\bar{Q}]$ (Ref. 19) is the elasticity matrix that, as noted earlier, will be different for the various plies in the facesheets as well as in the core.

Different through-thickness displacement models are adopted for the facesheets and the core. Thus, to develop the finite element representation, it is convenient to separate the sandwich plate into three parts: the bottom facesheet, the core, and the top facesheet. The aim in this separation is to carry out an analytical through-thickness integration with respect to z and, thereby, effectively reduce the model to two dimensions (x, y). In that regard, note that the reference surface for z is the sandwich plate, geometric middle surface.

As an alternative, each of the core, bottom and top facesheets could have its own reference surface; such a formulation would yield the same final result.

Bottom Facesheet

The strain energy for the bottom facesheet is

$$U_b = \frac{1}{2}\int_{vb} \{\bar{\sigma}\}\{\bar{\epsilon}\}^T \, \mathrm{d}v \tag{11}$$

where, because the facesheet is modeled as a Reissner–Mindlin plate, the stress–strain relation for each layer of the composite laminate takes the form

$$\begin{bmatrix} \sigma_{xx} \\ \sigma_{yy} \\ \sigma_{xz} \\ \sigma_{yz} \\ \sigma_{xy} \end{bmatrix}_k = \begin{bmatrix} \bar{Q}_{11} & \bar{Q}_{12} & 0 & 0 & \bar{Q}_{16} \\ & \bar{Q}_{22} & 0 & 0 & \bar{Q}_{26} \\ & & \bar{Q}_{44} & \bar{Q}_{45} & 0 \\ & & & \bar{Q}_{55} & 0 \\ \text{sym} & & & & \bar{Q}_{66} \end{bmatrix}_k \begin{bmatrix} \epsilon_x \\ \epsilon_y \\ \gamma_{yz} \\ \gamma_{xz} \\ \gamma_{xy} \end{bmatrix}_k \tag{12}$$

Using the displacement representation Eq. (1), the strain components become

$$\epsilon_{xx} = a_{0,x} + a_{1,x}z, \qquad \epsilon_{yy} = b_{0,y} + b_{1,y}z, \qquad \gamma_{yz} = b_1 + k_{0,y}$$

$$\gamma_{xz} = a_1 + k_{0,x}, \qquad \gamma_{xy} = (a_{0,y} + b_{0,x}) + (a_{1,y} + b_{1,x})z \tag{13}$$

where $(\,)_{,x}$ and $(\,)_{,y}$ indicate partial differentiation with respect to x and y, respectively.

The next step is to integrate the strain energy analytically with respect to z. Therefore, the strain energy in Eq. (9) is expressed in terms of $\{\bar{\epsilon}\}$ by substituting for $\{\bar{\sigma}\}$ from Eq. (12), and then the strains are expressed in terms of z based on the polynomial expressions in Eq. (13). After integration, the strain energy takes the form

$$U_b = \frac{1}{2}\int_x \int_y \{\bar{c}_b\}^T \{\bar{C}_b\}^T \begin{bmatrix} [A] & [B] & 0 \\ & [D] & 0 \\ \text{sym} & & [\bar{A}] \end{bmatrix} \{\bar{C}_b\}\{\bar{c}_b\} \, \mathrm{d}y \, \mathrm{d}x \tag{14}$$

where the operator matrix $\{\bar{C}_b\}$ is given in the Appendix and the vector of the polynomial coefficients is

$$\{\bar{c}_b\}^T = [a_0, a_1, b_0, b_1, k_0] \tag{15}$$

$$A_{ij} = \sum_{k=1}^{n} (\bar{Q}_{ij})_k (h_k - h_{k-1}), \qquad i, j = 1, 2, 6$$

$$B_{ij} = \frac{1}{2} \sum_{k=1}^{n} (\bar{Q}_{ij})_k \left(h_k^2 - h_{k-1}^2\right), \qquad i, j = 1, 2, 6$$

$$D_{ij} = \frac{1}{3} \sum_{k=1}^{n} (\bar{Q}_{ij})_k \left(h_k^3 - h_{k-1}^3\right), \qquad i, j = 1, 2, 6$$

$$\bar{A}_{ij} = \sum_{k=1}^{n} (\bar{Q}_{ij})_k (h_k - h_{k-1}), \qquad i, j = 4, 5 \tag{16}$$

where n is the number of plies in the facesheet and h_k and h_{k-1} are the upper and lower z coordinate of each ply.[19] This result looks very much like the standard result for laminated composite plates having terms depending on the first, second, and third degree of the thickness variable. However, there is one significant difference; that is, the reference plane is at the middle surface of the sandwich plate. Therefore, h_k and h_{k-1} are measured relative to that reference plane. This offset does not influence A_{ij} but does have a significant influence on B_{ij} and D_{ij}. With respect to B_{ij}, the most apparent effect is that even when the facesheet laminate is symmetric in the conventional sense B_{ij} does not vanish; symmetry is present only if the entire sandwich is symmetric. In that case the two facesheets are the mirror image of one another and the B_{ij} are the negative of one another and cancel only when the finite elements from the facesheets and core are assembled. The most significant effect of the offset is in the D_{ij}, which reflects the idea behind a sandwich structure.

The next step is to express the polynomial coefficients in the strain energy Eq. (14) in terms of the through-thickness nodal coefficients. With reference to Fig. 1, the required relationship is

$$\begin{bmatrix} a_0 \\ a_1 \\ b_0 \\ b_1 \\ k_0 \end{bmatrix} = \frac{1}{t_1 - t_0} \begin{bmatrix} -t_0 & t_1 & 0 & 0 & 0 \\ -1 & 1 & 0 & 0 & 0 \\ 0 & 0 & -t_0 & t_1 & 0 \\ 0 & 0 & -1 & 1 & 0 \\ 0 & 0 & 0 & 0 & t_1 - t_0 \end{bmatrix} \begin{bmatrix} u_1 \\ u_2 \\ v_1 \\ v_2 \\ w_2 \end{bmatrix} \tag{17}$$

where u_1, u_2, v_1, v_2, and w_2 are as shown in Fig. 1.

The final step is to introduce the (x, y) trial functions for u_1, u_2, v_1, v_2, and w_2; because this step is the same for both facesheets and the core, it will be presented for all three simultaneously later in this section.

Sandwich Core

The development for the core is similar to that presented earlier for the bottom facesheet.

The strain energy of the core is

$$U_c = \frac{1}{2} \int_c \{\bar{\sigma}\}\{\bar{\epsilon}\}^T \, \mathrm{d}v \tag{18}$$

whereas the stress–strain relation for each layer of the core takes the form

$$\begin{bmatrix} \sigma_{xx} \\ \sigma_{yy} \\ \sigma_{zz} \\ \sigma_{xz} \\ \sigma_{yz} \\ \sigma_{xy} \end{bmatrix}_k = \begin{bmatrix} \bar{Q}_{11} & \bar{Q}_{12} & \bar{Q}_{13} & 0 & 0 & \bar{Q}_{16} \\ & \bar{Q}_{22} & \bar{Q}_{23} & 0 & 0 & \bar{Q}_{26} \\ & & \bar{Q}_{33} & 0 & 0 & \bar{Q}_{36} \\ & & & \bar{Q}_{44} & \bar{Q}_{45} & 0 \\ & & & & \bar{Q}_{55} & 0 \\ \text{sym} & & & & & \bar{Q}_{66} \end{bmatrix}_k \begin{bmatrix} \epsilon_x \\ \epsilon_y \\ \epsilon_z \\ \gamma_{yz} \\ \gamma_{xz} \\ \gamma_{xy} \end{bmatrix}_k \tag{19}$$

Also, the strain-displacement representation follows from Eq. (2) as

$$\epsilon_{xx} = c_{0,x} + c_{1,x} z + c_{2,x} z^2 + c_{3,x} z^3$$

$$\epsilon_{yy} = d_{0,y} + d_{1,y} z + d_{2,y} z^2 + d_{3,y} z^3, \qquad \epsilon_{zz} = e_1 + 2e_2 z$$

$$\gamma_{yz} = \left(d_1 + 2d_2 z + 3d_3 z^2\right) + \left(e_{0,y} + e_{1,y} z + e_{2,y} z^2\right)$$

$$\gamma_{xz} = \left(c_1 + 2c_2 z + 3c_3 z^2\right) + \left(e_{0,x} + e_{1,x} z + e_{2,x} z^2\right)$$

$$\gamma_{xy} = \left(c_{0,y} + c_{1,y} z + c_{2,y} z^2 + c_{3,y} z^3\right) + \left(d_{0,x} + d_{1,x} z + d_{2,x} z^2 + d_{3,x} z^3\right) \tag{20}$$

Substituting the various expressions into the strain energy and integrating with respect to z yields the desired result:

$$U_c = \frac{1}{2} \int_x \int_y \{\bar{c}_c\}^T \{\bar{C}_c\}^T \begin{bmatrix} [A] & [B] & [D] & [E] \\ & [D] & [E] & [F] \\ & & [F] & [G] \\ \text{sym} & & & [H] \end{bmatrix} \{\bar{C}_c\}\{\bar{c}_c\} \, \mathrm{d}y \, \mathrm{d}x \tag{21}$$

where the operator matrix $\{\bar{C}_c\}$ is given in the Appendix and

$$\{\bar{c}_c\}^T = [c_0, c_1, c_2, c_3, d_0, d_1, d_2, d_3, e_0, e_1, e_2] \tag{22}$$

$$A_{ij} = \sum_{k=1}^{n} (\bar{Q}_{ij})_k (h_k - h_{k-1}), \qquad i, j = 1, 6$$

$$B_{ij} = \frac{1}{2} \sum_{k=1}^{n} (\bar{Q}_{ij})_k \left(h_k^2 - h_{k-1}^2\right), \qquad i, j = 1, 6$$

$$D_{ij} = \frac{1}{3} \sum_{k=1}^{n} (\bar{Q}_{ij})_k \left(h_k^3 - h_{k-1}^3\right), \qquad i, j = 1, 6$$

$$E_{ij} = \frac{1}{4} \sum_{k=1}^{n} (\bar{Q}_{ij})_k \left(h_k^4 - h_{k-1}^4\right), \qquad i, j = 1, 6$$

$$F_{ij} = \frac{1}{5} \sum_{k=1}^{n} (\bar{Q}_{ij})_k \left(h_k^5 - h_{k-1}^5\right), \qquad i, j = 1, 6$$

$$G_{ij} = \frac{1}{6} \sum_{k=1}^{n} (\bar{Q}_{ij})_k \left(h_k^6 - h_{k-1}^6\right), \qquad i, j = 1, 6$$

$$H_{ij} = \frac{1}{7} \sum_{k=1}^{n} (\bar{Q}_{ij})_k \left(h_k^7 - h_{k-1}^7\right), \qquad i, j = 1, 6 \tag{23}$$

Note that there is coupling of higher order: B, D, E, F, G, and H. Also, even-ordered coupling terms will vanish for a symmetric core if the facesheets are of equal thickness; however, even then there are still higher-order coupling terms: D, F, and H. As may be seen, the highest-order terms involve the thickness variable raised to the seventh power.

Again it is necessary to express the polynomial coefficients in the strain energy Eq. (21) in terms of through-thickness nodal coefficients. With reference to Fig. 1 the required relationships are

$$\begin{bmatrix} c_0 \\ c_1 \\ c_2 \\ c_3 \end{bmatrix} = \frac{1}{16} \begin{bmatrix} -1 & 9 & 9 & -1 \\ 1/t_0 & -27/t_0 & 27/t_0 & -1/t_0 \\ 9/t_0^2 & -9/t_0^2 & -9/t_0^2 & 9/t_0^2 \\ -9/t_0^3 & 27/t_0^3 & -27/t_0^3 & 9/t_0^3 \end{bmatrix} \begin{bmatrix} u_2 \\ u_3 \\ u_5 \\ u_6 \end{bmatrix} \tag{24}$$

$$\begin{bmatrix} d_0 \\ d_1 \\ d_2 \\ d_3 \end{bmatrix} = \frac{1}{16} \begin{bmatrix} -1 & 9 & 9 & -1 \\ 1/t_0 & -27/t_0 & 27/t_0 & -1/t_0 \\ 9| t_0^2 & -9| t_0^2 & -9| t_0^2 & 9| t_0^2 \\ -9| t_0^3 & 27| t_0^3 & -27| t_0^3 & 9| t_0^3 \end{bmatrix} \begin{bmatrix} v_2 \\ v_3 \\ v_5 \\ v_6 \end{bmatrix} \tag{25}$$

$$\begin{bmatrix} e_0 \\ e_1 \\ e_2 \end{bmatrix} = \frac{1}{16} \begin{bmatrix} 0 & 1 & 1 \\ 1/2t_0 & 0 & -1/2t_0 \\ 1| 2t_0^2 & 0 & 1| 2t_0^2 \end{bmatrix} \begin{bmatrix} w_2 \\ w_4 \\ w_6 \end{bmatrix} \tag{26}$$

where $u_2, \ldots, v_2, \ldots, w_2, \ldots$ are shown in Fig. 1.

Note that, in the actual implementation, the three relations just given are combined into one expression; the preceding form was used for presentation purposes.

Top Facesheet

The formulation for the top facesheet parallels that of the bottom facesheet and will, therefore, be presented quite briefly. The strain energy is

$$U_t = \frac{1}{2} \int_{vt} \{\bar{\sigma}\}\{\bar{\epsilon}\}^T \, dv \tag{27}$$

where the stress–strain relation for each composite layer takes the form of Eq. (12). Using the earlier presented displacement representation [Eq. (3)], the strain components become

$$\begin{aligned} \epsilon_{xx} &= f_{0,x} + f_{1,x} z, & \epsilon_{yy} &= g_{0,y} + g_{1,y} z \\ \gamma_{yz} &= g_1 + h_{0,y}, & \gamma_{xz} &= f_1 + h_{0,x} \\ \gamma_{xy} &= (f_{0,y} + g_{0,x}) + (f_{1,y} + g_{1,x}) z \end{aligned} \tag{28}$$

Making the appropriate substitutions and integrating with respect to z yield

$$U_t = \frac{1}{2} \int_x \int_y \{\bar{c}_t\}^T \{\bar{C}_t\}^T \begin{bmatrix} [A] & [B] & 0 \\ & [D] & 0 \\ \text{sym} & & [\bar{A}] \end{bmatrix} \{\bar{C}_t\}\{\bar{c}_t\} \, dy \, dx \tag{29}$$

where the operator matrix $\{\bar{C}_t\}$ is given in the Appendix and the vector of the polynomial coefficients is

$$\{\bar{c}_{tf}\}^T = [f_0, f_1, g_0, g_1, h_0] \tag{30}$$

Expressing the polynomial coefficients in terms of through-thickness nodal coefficients yields

$$\begin{bmatrix} f_0 \\ f_1 \\ g_0 \\ g_1 \\ h_0 \end{bmatrix} = \frac{1}{t_2 - t_0} \begin{bmatrix} t_2 & -t_0 & 0 & 0 & 0 \\ -1 & 1 & 0 & 0 & 0 \\ 0 & 0 & t_2 & -t_0 & 0 \\ 0 & 0 & -1 & 1 & 0 \\ 0 & 0 & 0 & 0 & t_2 - t_0 \end{bmatrix} \begin{bmatrix} u_6 \\ u_7 \\ v_6 \\ v_7 \\ w_6 \end{bmatrix} \tag{31}$$

where u_6, u_7, v_6, v_7, and w_6 are as shown in Fig. 1.

In-Plane Modeling

Because the preceding energy expressions have been integrated with respect to z, the problem has been reduced to a two-dimensional problem in the 15 nodal parameters u_1, u_2, u_3, u_5, u_6, u_7, v_1, v_2, v_3, v_5, v_6, v_7, w_2, w_4, and w_6. The representation of the through-thickness modeling in terms of these 15 parameters allows a straightforward assembly of the contributions from the facesheets and the core that is typical of finite element procedures. Therefore, every node has the 15 nodal parameters as nodal degrees of freedom; that is, from the point of view of the analysis, the 7 through-thickness nodes have effectively collapsed into a single node lying at the plate middle surface. The preceding matrices and relations are the starting point for the in-plane two-dimensional finite element analysis. The in-plane (x, y) trial functions for the u, v, and w nodal coefficients are taken as bicubic Lagrange polynomials based on the excellent performance of such elements.[18] Each bicubic element when fully assembled has 112 nodes and 240 degrees of freedom, and the corresponding element stiffness matrices and element consistent force vectors are generated following standard finite element procedures. Numerical integration uses fourth-order Gauss-quadrature that provides exact integration of the strain energy expressions. From an implementation point of view, assembly of the global matrices is done in a two-step procedure. In the first step the element contributions from the top and bottom facesheets and the core are calculated separately as subelement stiffness matrices and are then assembled through the thickness to yield the full element matrix. The second step involves the assembly of these full element matrices to form the global stiffness matrix. A similar approach is used for the global force vector.

IV. Numerical Examples

Based on the described model, a finite element code was developed that allows any combination of applied loads, boundary conditions, and material properties, that is, very soft core material, isotropic, anisotropic, high stiffness, etc. The code was tested extensively to verify correctness and accuracy using a range of comparison problems: rigid-body motion, strain energy convergence, uniformly distributed in-plane loads, uniform lateral load, and convergence to classical plate theory results for thin plates. All tests showed excellent results. To illustrate the formulation capabilities, two example problems of sandwich plates loaded by concentrated forces are presented here; both cases are selected from the recent works by others[11,16] and are problems of particular interest for sandwich plates. An example of a sandwich plate subjected to a uniform load can be found in previous publications by the present authors.[20,21]

Concentrated Load: Thybo Thomsen Problem

To illustrate the capabilities of this formulation, a comparison to the results of work presented by Thybo Thomsen[16] was undertaken inasmuch as it provides an excellent means of fully evaluating the element capabilities. The problem of interest is a sandwich plate subjected to a concentrated load on the top facesheet. The geometry and boundary conditions are shown in Fig. 2; geometric and load symmetry means only a quarter of plate need be analyzed. The plate geometry and material characteristics are summarized in Table 1.

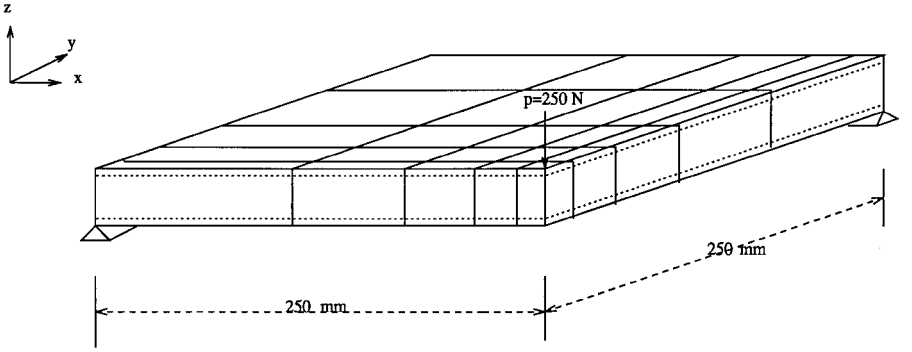

Fig. 2 Sandwich plate subjected to point load.

Table 1 Plate description: Thybo Thomsen problem

Parameter	Value
Plate dimensions	500 × 500 mm
Thicknesses	
Core	30.0 mm
Facesheets	3.0 mm
Material properties	
Core	E_c = 0.1 GPa, ν_c = 0.35
Facesheets	E_{11} = 33.6 GPa, E_{22} = 8.4 GPa
	ν_{12} = 0.32, G_{12} = 3.1 GPa
Concentrated load	P = 1000.0 N

Table 2 Plate description: Frostig problem

Parameter	Value
Plate dimensions	300 × 300 mm
Thicknesses	
Core	19.1 mm
Facesheets	0.5 mm
Material properties	
Core	E_c = 52.5 MPa, ν_c = 0.3
Facesheets	E_{11} = E_{22} = 27.4 GPa
	ν_{12} = 0.3, G_{12} = 1.6 GPa
Concentrated load	P = 50.0 kg

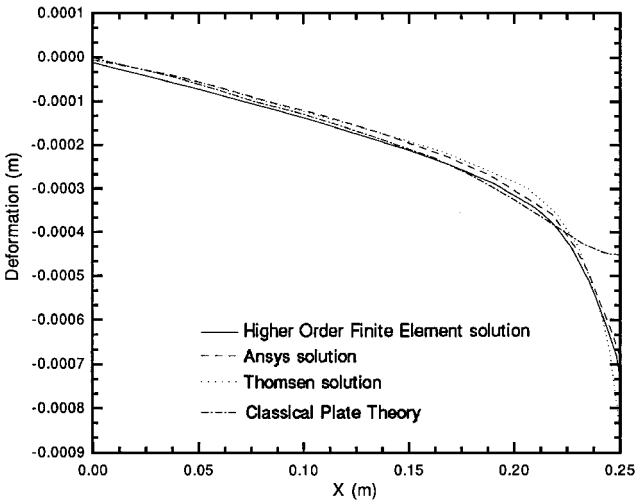

Fig. 3 Top facesheet deformation w: Thybo Thomsen problem.

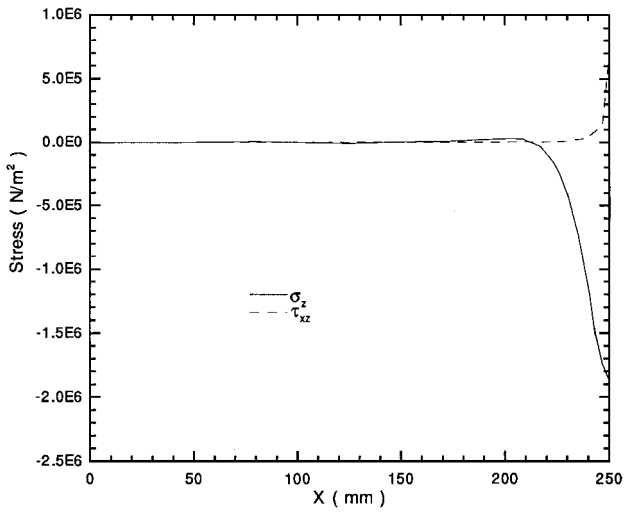

Fig. 4 Core/top facesheet interface stress distribution: Thybo Thomsen problem.

As the finite element mesh was refined, the solution converged very quickly, and it was found that a 5 × 5 mesh provided excellent accuracy. All of the results to follow are presented along the plate centerline: $0 \leq x \leq 250$, $y = 250$. The deflection of the top facesheet is presented in Fig. 3; the results of the Thybo Thomsen solution and ANSYS finite element are presented for comparison. In addition, Fig. 4 shows the distribution of the peel and shear stresses at the interface between the core and the top facesheet and Fig. 5 presents the in-plane σ_x at the upper and lower surface of the top facesheet.

Comparing the present results with those of Ref. 16 reveals the capability of the current model. The maximum deflection of the top facesheet as predicted by the present model in Fig. 3 lies between the maximum presented by elastic foundation model and the ANSYS finite element analysis of Thybo Thomsen's work. In this ANSYS

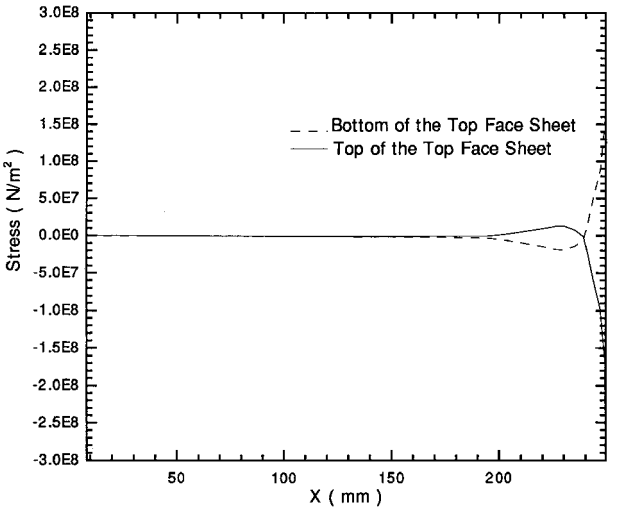

Fig. 5 Top facesheet in-plane stress σ_x: Thybo Thomsen problem.

model, 1800 isoparametric eight-node solid elements with three translational degrees of freedom at each node were used. As can be seen, even with the very large number of elements, the deflection results are less than those of the present model, and because both analyses are displacement based, it may be inferred that the current results are more accurate. It is felt the differences result from the use of linear elements that yields the stiffer behavior.

Concentrated Load: Frostig Problem

As a second example, a comparison to the analysis by Frostig et al.[11] of a sandwich plate loaded by concentrated force on the top facesheet is undertaken. Because of the similarity with the Thybo Thomsen problem, the geometry and boundary conditions of the sandwich plate are not illustrated. The plate description for this example is given in Table 2.

Again, with mesh refinement, the solution converged very quickly, and it was found that a 5 × 5 mesh provided excellent accuracy. Results are presented along the plate centerline: $0 \leq x \leq 150$, $y = 150$.

Calculated deflections of the top and bottom facesheets are compared with the reference results in Fig. 6. Excellent agreement between the present and reference results may be observed with the exception of the bottom sheet deflection under the point of load application. From physical considerations it would seem that the reference result may be unrealistic. Figure 7 shows the distribution of the peel stress at different locations through the core, and Figs. 8 and 9 presents the shear stress distribution in the core. In all previous models, because of the omission of the in-plane core stiffness, core stresses in the x and y directions vanish. This is not the case in the present approach, and these stresses are presented in Figs. 10 and 11, respectively. Note that in the region of the point of load these stress components vary rapidly and assume quite large values. The in-plane stresses at the top and bottom of the top facesheet are presented in Figs. 12 and 13, and the significant influence of localized bending near the load application point is to be noted.

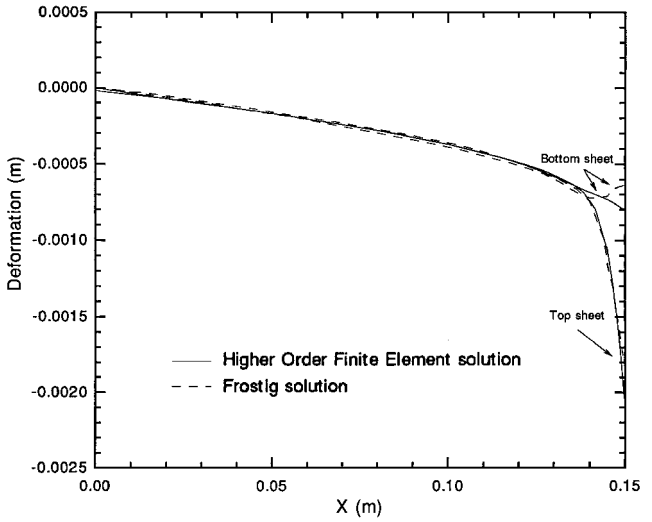

Fig. 6 Top and bottom facesheet deformation w: Frostig problem.

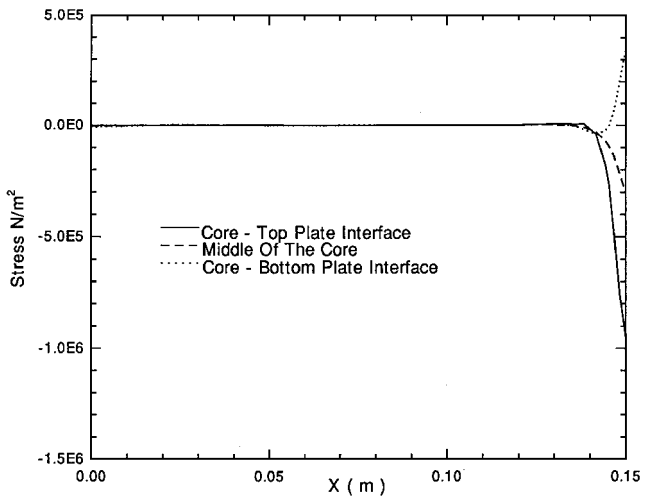

Fig. 7 Core peel stress σ_z: Frostig problem.

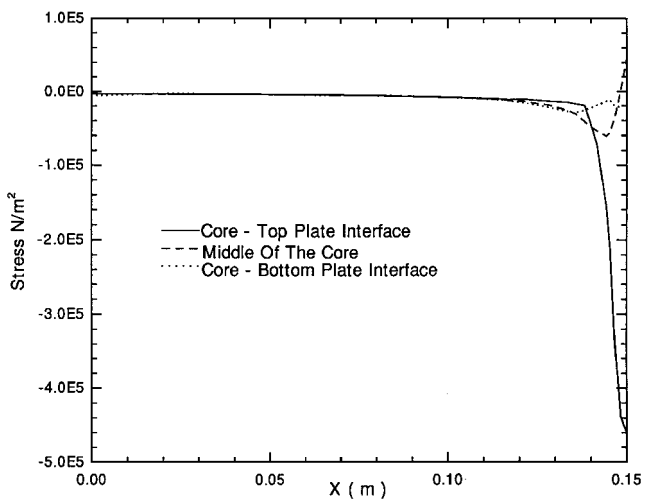

Fig. 8 Core shear stress τ_{xz}: Frostig problem.

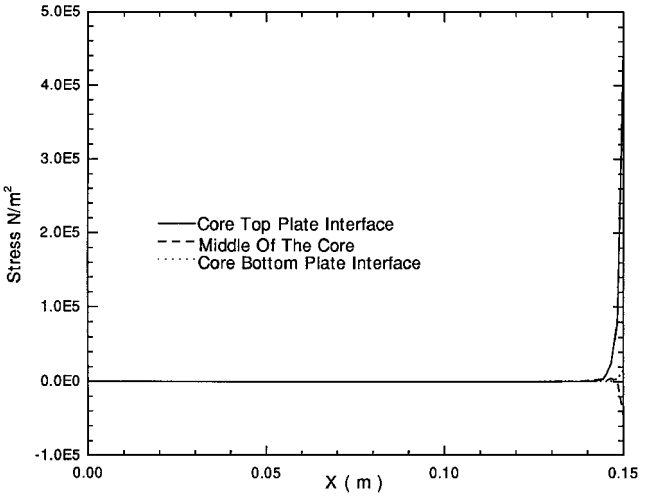

Fig. 9 Core shear stress τ_{yz}: Frostig problem.

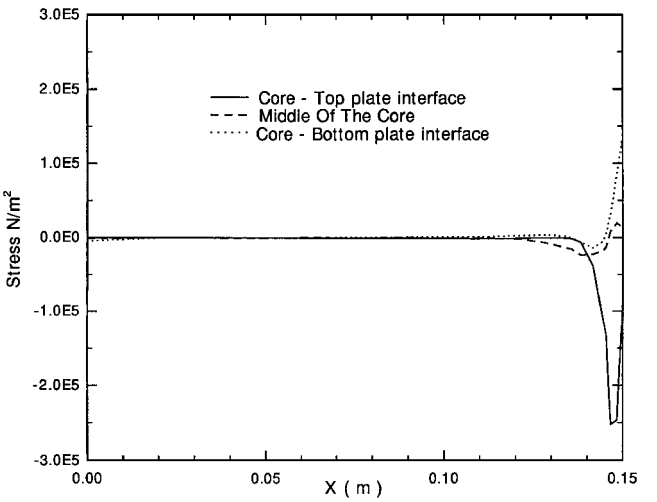

Fig. 10 Core in-plane stress σ_x: Frostig problem.

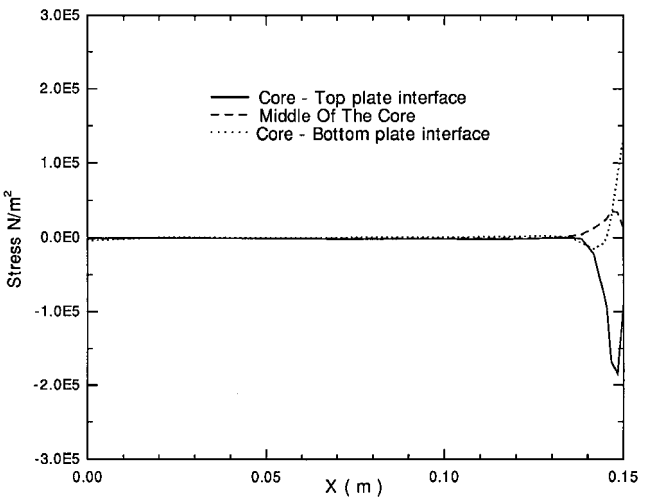

Fig. 11 Core in-plane stress σ_y: Frostig problem.

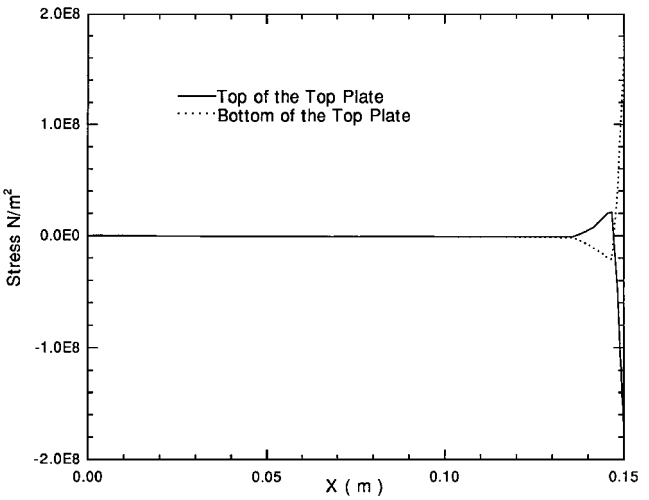

Fig. 12 Top facesheet in-plane stress σ_x: Frostig problem.

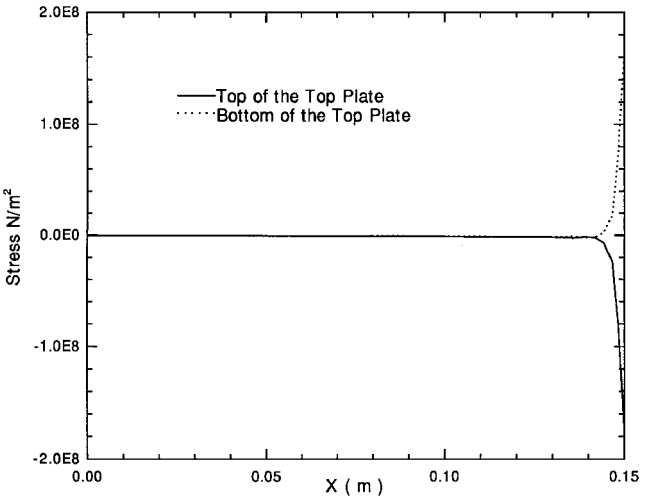

Fig. 13 Top facesheet in-plane stress σ_y: Frostig problem.

V. Conclusions

The presented model provides an accurate and robust tool for the analysis of sandwich plate response. Because Reissner–Mindlin plate theory has been used to model the facesheets, shear deformation of the facesheets is explicitly included in the analysis, and this allows a continuous distribution of transverse shear stress across the plate thickness. The three-dimensional representation used to model the core response is thought to capture the important characteristics of the core; therefore, it is felt this allows a good model of the physical problem. Finally, example calculations illustrate that the solution converges very quickly and gives very good results even with a small number of elements.

Appendix: Operator Matrices

The operator matrix $\{\bar{C}_b\}$ is given by

$$\{\bar{C}_b\} = \begin{bmatrix} ()_{,x} & 0 & 0 & 0 & 0 \\ 0 & 0 & ()_{,y} & 0 & 0 \\ ()_{,y} & 0 & ()_{,x} & 0 & 0 \\ 0 & ()_{,x} & 0 & 0 & 0 \\ 0 & 0 & 0 & ()_{,y} & 0 \\ 0 & ()_{,y} & 0 & ()_{,x} & 0 \\ 0 & 0 & 0 & 1 & ()_{,y} \\ 0 & 1 & 0 & 0 & ()_{,x} \end{bmatrix} \tag{A1}$$

The operator matrix $\{\bar{C}_c\}$ is given by

$$\{\bar{C}_c\} = \begin{bmatrix} ()_{,x} & 0 & 0 & 0 & 0 & 0 & 0 & 0 & 0 & 0 & 0 \\ 0 & 0 & 0 & 0 & ()_{,y} & 0 & 0 & 0 & 0 & 0 & 0 \\ 0 & 0 & 0 & 0 & 0 & 0 & 0 & 0 & 0 & 1 & 0 \\ 0 & 0 & 0 & 0 & 0 & 1 & 0 & 0 & ()_{,y} & 0 & 0 \\ 0 & 1 & 0 & 0 & 0 & 0 & 0 & 0 & ()_{,x} & 0 & 0 \\ ()_{,y} & 0 & 0 & 0 & ()_{,x} & 0 & 0 & 0 & 0 & 0 & 0 \\ 0 & ()_{,x} & 0 & 0 & 0 & 0 & 0 & 0 & 0 & 0 & 0 \\ 0 & 0 & 0 & 0 & 0 & ()_{,y} & 0 & 0 & 0 & 0 & 0 \\ 0 & 0 & 0 & 0 & 0 & 0 & 0 & 0 & 0 & 0 & 2 \\ 0 & 0 & 0 & 0 & 0 & 0 & 2 & 0 & 0 & ()_{,y} & 0 \\ 0 & 0 & 2 & 0 & 0 & 0 & 0 & 0 & 0 & ()_{,x} & 0 \\ 0 & ()_{,y} & 0 & 0 & 0 & ()_{,x} & 0 & 0 & 0 & 0 & 0 \\ 0 & 0 & ()_{,x} & 0 & 0 & 0 & 0 & 0 & 0 & 0 & 0 \\ 0 & 0 & 0 & 0 & 0 & 0 & ()_{,y} & 0 & 0 & 0 & 0 \\ 0 & 0 & 0 & 0 & 0 & 0 & 0 & 0 & 0 & 0 & 0 \\ 0 & 0 & 0 & 0 & 0 & 0 & 0 & 3 & 0 & 0 & ()_{,y} \\ 0 & 0 & 0 & 3 & 0 & 0 & 0 & 0 & 0 & 0 & ()_{,x} \\ 0 & 0 & ()_{,y} & 0 & 0 & 0 & ()_{,x} & 0 & 0 & 0 & 0 \\ 0 & 0 & 0 & ()_{,x} & 0 & 0 & 0 & 0 & 0 & 0 & 0 \\ 0 & 0 & 0 & 0 & 0 & 0 & 0 & ()_{,y} & 0 & 0 & 0 \\ 0 & 0 & 0 & 0 & 0 & 0 & 0 & 0 & 0 & 0 & 0 \\ 0 & 0 & 0 & 0 & 0 & 0 & 0 & 0 & 0 & 0 & 0 \\ 0 & 0 & 0 & 0 & 0 & 0 & 0 & 0 & 0 & 0 & 0 \\ 0 & 0 & 0 & ()_{,y} & 0 & 0 & 0 & ()_{,x} & 0 & 0 & 0 \end{bmatrix} \tag{A2}$$

The operator matrix $\{\bar{C}_t\}$ is given by

$$\{\bar{C}_t\} = \begin{bmatrix} ()_{,x} & 0 & 0 & 0 & 0 \\ 0 & 0 & ()_{,y} & 0 & 0 \\ ()_{,y} & 0 & ()_{,x} & 0 & 0 \\ 0 & ()_{,x} & 0 & 0 & 0 \\ 0 & 0 & 0 & ()_{,y} & 0 \\ 0 & ()_{,y} & 0 & ()_{,x} & 0 \\ 0 & 0 & 0 & 1 & ()_{,y} \\ 0 & 1 & 0 & 0 & ()_{,x} \end{bmatrix} \tag{A3}$$

References

[1] Potter, K., *An Introduction to Composite Products*, Chapman and Hall, New York, 1997, pp. 111–120.

[2] Reissner, E., "Finite Deflection of Sandwich Plates," *Journal of Aerospace Science*, Vol. 15, No. 7, 1948, pp. 435–440.

[3] Allen, H. G., *Analysis and Design of Structural Sandwich Panels*, Pergamon, London, 1969, pp. 8–25.

[4] Plantema, F. J., *Sandwich Construction*, Wiley, New York, 1966, pp. 55–77.

[5] Holt, D. J., and Webber, J. P. H., "Exact Solution to Some Honeycomb Sandwich Beam, Plate and Shell Problems," *Journal of Strain Analysis*, Vol. 17, No. 1, 1982, pp. 1–8.

[6] Pearce, T. R. A., "The Stability of Simply-Supported Sandwich Panels with Fibre Reinforced Face Plates," Ph.D. Dissertation, Dept. of Mechanical Engineering, Univ. of Bristol, Bristol, England, U.K., 1973.

[7] Monforton, G. R., and Ibrahim, I. M., "Modified Stiffness Formulation of Unbalanced Anisotropic Sandwich Plates," *International Journal of Mechanical Science*, Vol. 19, No. 6, 1977, pp. 335–343.

[8] Ojalvo, I. V., "Departures from Classical Beam Theory in Laminated Sandwich and Short Beams," *AIAA Journal*, Vol. 15, No. 10, 1977, pp. 1518–1521.

[9] Frostig, Y., Baruch, M., Vilnay, O., and Sheinman, I., "Bending of Non-Symmetric Sandwich Beam with Transversely Flexible Core," *Journal of Engineering Mechanics*, Vol. 117, No. 9, 1991, pp. 1931–1952.

[10] Frostig, Y., Baruch, M., Vilnay, O., and Sheinman, I., "High of ^{11}-Order Theory for Sandwich-Beam Behaviour with Transversely Flexible Core," *Journal of Engineering Mechanics*, Vol. 118, No. 5, 1992, pp. 1026–1043.

[11] Frostig, Y., and Baruch, M., "Higher-Order Bending of Sandwich Panels with a Transversely Flexible Core," AIAA Paper 94-1394, April 1994.

[12] Frostig, Y., and Baruch, M., "Localized Loads Effects in High-Order Bending of Sandwich Panels with Flexible Core," *Journal of Engineering Mechanics*, Vol. 122, No. 11, 1996, pp. 1069–1076.

[13] Reddy, J. N., *Energy and Variational Methods in Applied Mechanics*, Wiley, New York, 1984, pp. 401–404.

[14] Reddy, J. N., "A Review of Refined Theories of Laminated Composite Plates," *Shock and Vibration Digest*, Vol. 22, No. 7, 1990, pp. 3–17.

[15] Robbins, D. H., and Reddy, J. N., "Modelling of Thick Composites Using a Layer Wise Laminate Theory," *International Journal for Numerical Methods in Engineering*, Vol. 36, No. 4, 1993, pp. 665–677.

[16] Thybo Thomsen, O., "Analysis of Local Bending Effects in Sandwich Plates with Orthotropic Face Layers Subjected to Localised Loads," *Composite Structures*, Vol. 25, No. 1–4, 1993, pp. 511–520.

[17] Thybo Thomsen, O., "Analysis of Sandwich Panels with Through-the-Thickness Inserts Using a Higher-Order Sandwich Plate Theory," European Space Research and Technology Center, Rept. EWP-1807, Noordwijk, The Netherlands, 1994.

[18] Heppler, G. R., and Hansen, J. S., "A Mindlin Element for Thick and Deep Shells," *Computer Methods in Applied Mechanics and Engineering*, Vol. 54, No. 1, 1986, pp. 21–27.

[19] Jones, R. M., *Mechanics of Composite Materials*, Hemisphere, New York, 1975, pp. 148–171.

[20] Oskooei, S., and Hansen, J. S., "A Higher Order Finite Element for Sandwich Plates," AIAA Paper 98-1717, April 1998.

[21] Oskooei, S., and Hansen, J. S., "A Higher Order Finite Element for Sandwich Plate Analysis," Inst. of Mechanical Engineering, Rept. 93, Aalborg Univ., Aalborg, Denmark, 1998.

R. K. Kapania
Associate Editor